Molecular Vision 2021; 27:494-505 <http://www.molvis.org/molvis/v27/494>
Received 2 May 2020 | Accepted 30 August 2021 | Published 1 September 2021

© 2021 Molecular Vision

Comparative proteome analysis of form-deprivation myopia in sclera with iTRAQ-based quantitative proteomics

Ying Yuan,[1,2,3] Chengcheng Zhu,[1,3,4] Mingming Liu,[1,3,5] Bilian Ke[1,2,3]

[1]Department of Ophthalmology, Shanghai General Hospital, Shanghai Jiao Tong University School of Medicine; Shanghai, China; [2]National Clinical Research Center for Eye Diseases; Shanghai, China; [3]Shanghai Key Laboratory of Fundus Disease, Shanghai, China; [4]Shanghai engineering center for visual science and photomedicine, Shanghai, China; [5]Shanghai engineering center for precise diagnosis and treatment of eye diseases, Shanghai, China

Objective: Scleral remodeling plays a key role in axial elongation in myopia. The aim of the present study was to identify the proteomics changes and specific signaling networks to gain insight into the molecular basis of scleral remodeling in myopic eyes.

Methods: Guinea pig form-deprivation myopia was induced with a translucent diffuser on a random eye for 4 weeks, while the other eye served as the contralateral control group. The axial length and refraction were measured at the beginning and end of the treatment. The proteins were extracted from the sclerae of each group and prepared for quantitative isobaric tags for relative and absolute quantification (iTRAQ) labeling combined with liquid chromatography-tandem mass spectrometry (LC−MS/MS) analysis. The coexpression networks and protein functions were analyzed using Gene Ontology (GO) and Ingenuity Pathway Analysis (IPA). Quantitative real-time PCR (qRT-PCR) and western blotting were performed to confirm the authenticity and accuracy of the iTRAQ results.

Results: After 4 weeks, the form-deprivation eyes developed significant degrees of myopia, and the axial length increased statistically significantly ($p<0.05$). A total of 2,579 unique proteins with <1% false discovery rate (FDR) were identified. Furthermore, 56 proteins were found to be upregulated, and 84 proteins were found to be downregulated, with a threshold of a 1.2-fold change and $p<0.05$ in the myopia group, when compared to the control group. Further bioinformatics analysis indicated that 44 of 140 differentially expressed proteins were involved in cellular movement and cellular assembly and organization. The qRT-PCR or western blotting results confirmed that myosin IIB, ACTIN3, and cellular cytoskeletons were downregulated, while RhoA and RAP1A were upregulated in the sclera in myopic eyes. These results were consistent with the proteomics results.

Conclusions: Proteomics and bioinformatics results can be helpful for identifying proteins and providing new insights for better understanding of the molecular mechanism underlying scleral remodeling. These results revealed that the proteins associated with cellular movement and cellular assembly and organization are altered during the development of myopia. Furthermore, RhoA plays a key role in the pathways involved in cellular movement and cellular assembly and organization.

Myopia is one of the most common visual disorders with increasing occurrence, especially in some East Asian countries [1,2]. This has been characterized by the excessive axial elongation of the eye, which causes images to focus in front of the retina. The sclera, which is the outer layer of the eye, critically determines the eye size, as well as the refractive status of the eye. It has been well documented that structural and biomechanical changes occur in the sclera in myopic eyes. Humans and animals with high myopia have been shown to have thinner sclera, when compared to emmetropic eyes [3,4]. Furthermore, an increase in creep rate and a decrease in biomechanical stability were found in sclera tissues obtained from eyes with myopia [5,6]. These biomechanical changes cause the sclera to have less resistance to expansion in response to normal intraocular pressures, thus facilitating the elongation of the eye in myopia [7].

The sclera is predominantly made up of the extracellular matrix (ECM) and interspersed fibroblasts. The ECM mainly comprises collagen, with type I collagen showing the highest expression among the numerous collagen subtypes [8,9]. Studies conducted on experimental models of myopia have unraveled a variety of factors involved in scleral ECM remodeling during the development of myopia. It has been reported that there is increased degradation and reduced synthesis of type I collagens during the development of myopia [10]. In addition, the sclera has been shown to undergo reduced expression of glycosaminoglycan and proteoglycan [11,12]. Apart from these ECM content changes, the collagen fibril diameter also decreased [13,14]. Taken together, these biologic changes render the sclera structurally thinner and

Correspondence to: Bilian Ke, Department of Ophthalmology, Shanghai General Hospital, Shanghai Jiao Tong University School of Medicine, 100 Haining Road Shanghai 200080, China; Phone: +86-21-63243071; FAX: ??; email: kebilian@126.com

biomechanically weaker. Scleral fibroblasts are able to maintain the ECM by secreting various proteinases and cytokines. Higher levels of MMP-2 and decreased levels of TIMP-1 have also been found in the sclera in myopic eyes [15]. These molecular changes can activate the breakdown of collagen and proteoglycans. The downregulation of TGF-β isoforms, particularly TGF-β1, and the upregulation of FGF receptor-1 have been observed during the development of myopia, which may be correlated to the reduced synthesis of collagens [16,17]. The biologic changes found in these studies merely represent the important roles of a few selected scleral proteins in the development of myopia. However, the entire profile of scleral proteins involved in form-deprivation myopia (FDM) remains to be confirmed.

Proteomics has been widely used to identify differentially expressed proteins in various diseases, providing insights into the underlying molecular mechanisms. In the myopia model, scleral tissues from the tree shew and chick have been examined using the two-dimensional gel electrophoresis (2DGE) approach [18,19]. At present, isobaric tag for relative and absolute quantification (iTRAQ)-based quantitative proteomics has facilitated the detection of low-abundance and low-molecular weight proteins, and improved the sensitivity of proteome screening [20,21]. To date, few reports have identified the differentially expressed proteins in myopia with iTRAQ quantitative proteomics. Veluchamy and colleagues used the iTRAQ proteomics strategy to demonstrate the importance of the retina GABA pathway in the development of myopia [22]. However, comprehensive sclera iTRAQ proteomics and bioinformatic analysis in guinea pig eyes with myopia have not been reported. In the present study, we performed an iTRAQ proteomics study of the sclera in myopic eyes, aiming to provide novel insights into scleral remodeling in the development of myopia. Furthermore, bioinformatic analysis provides an important bioinformatic resource for the underlying mechanism in scleral remodeling in myopic eyes.

METHODS

Experimental design: In the present study, all procedures complied with the ARVO Statement for the Use of Animals in Ophthalmic and Vision Research and were approved by the Ethics Committee of Shanghai General Hospital, Shanghai Jiao Tong University School of Medicine. Pigmented guinea pigs (2 weeks old) were reared under a 12 h:12 h light-dark cycle in the laboratory animal center (male and female). The random eye was treated with a translucent diffuser for 4 weeks, while the other eye that did not receive any treatment was assigned to the contralateral control group.

The refractive errors were measured using an automated infrared photorefractor. For each eye, an average of ten measurements was recorded, and the mean was used for the statistical analysis. The axial length (AL) was measured using A-scan ultrasonography (Strong 6000A, Wuhan, China) under topical anesthesia (0.4% oxybuprocaine hydrochloride). The ultimate AL was the average of eight independent measurements.

Sample preparation: Scleral tissues in the control and form-deprivation groups were harvested. These collected tissues were ground into a fine powder in liquid nitrogen and extracted with lysis buffer (pH 7.6) containing 4% sodium dodecyl sulfate (SDS), 100 mM of Tris-HCl, and 1 mM of dithiothreitol (DTT). Then, the suspension was sonicated at 80 W on ice ten times (10 s at a time with 15-s intervals). After centrifugation at 14,000 ×*g* for 40 min at 4 °C, the supernatants were collected, dried, and stored at −80 °C for further use. The concentration of protein was determined with bicinchoninic acid (BCA) assay (P0011, Beyotime biotechnology, Shanghai, China). After separation with electrophoresis on 12.5% SDS-polyacrylamide gels, the protein samples (20 μg) were stained with Coomassie brilliant blue to confirm the parallelisms among the samples.

Protein digestion and iTRAQ labeling: The proteins were digested using the filter-aided sample preparation (FASP) procedure. Briefly, each sample of 300 μg of proteins was mixed with 100 mM of DTT buffer. Then, 200 μl of UA buffer (8 M of urea, 150 mM of Tris-HCl, pH 8.0) was added. Afterward, the mixture was transferred to a 10-kDa centrifugal filter (Sartorius, Gottingen, Germany) and centrifuged twice at 14,000 ×*g* for 15 min. Then, 100 μl of 100 mM of iodoacetamide in UA buffer was added, and the samples were incubated in the dark for 30 min. The filters were washed with 100 μl of UA buffer twice and then washed twice with 100 μl of dissolution buffer. Then, the protein samples were digested with 4 μg of trypsin (Promega, Madison, WI) in 40 μl of dissolution buffer overnight at 37 °C. On the following day, the samples were centrifuged at 14,000 ×*g* for 15 min. The resulting peptides were transferred to new tubes. The peptide content was measured with ultraviolet (UV) light spectral density at 280 nm. Then, 100 μg of peptide from each sample was labeled using 8-plex iTRAQ reagents, according to the manufacturer's instructions and as previously described (AB Sciex, Framingham, MA). Three samples from the control group were labeled with iTRAQ tags 113, 114, and 115. The other three samples from the FDM group were labeled with iTRAQ tags 116, 117, and 118.

Peptide fractionation with SCX chromatography: The iTRAQ-labeled peptides were fractionated with strong cation

exchange (SCX) chromatography using the AKTA Purifier 100 system (GE Healthcare, Chicago, IL). The vacuum-dried peptide mixture was reconstituted with buffer A (10 mM of KH_2PO_4 in 25% ACN, pH 3.0) and loaded onto a 4.6 × 100 mm PolySULFOETHYL column (5 µm, 200 Å; PolyLC Inc., Columbia, MD). Then, the peptides were eluted at a flow rate of 1 ml/min with a gradient of 0–8% buffer B (500 mM of KCl, 10 mM of KH_2PO_4 in 25% of ACN, pH 3.0) for 22 min, a gradient of 8–52% buffer B for 25 min, a gradient of 52–100% buffer B for 3 min, and a gradient of 100% buffer B for 8 min. The elution was detected by measuring the absorbance at 214 nm, and the fractions were collected every 1 min. A total of 30 fractions were collected, pooled, and desalted on C18 Cartridges (66872-U Sigma).

Reverse phase LC-MS/MS analysis: The lyophilized peptides were reconstituted in 0.1% formic acid. Liquid chromatography was performed using the nano- high performance liquid chromatography (HPLC) system (EASY-nLC, Thermo Scientific, Waltham, MA). A total of 10 µl of supernatant was loaded on the C18 trap column (3 µm, nanoViper C18, 100 Å, 100 µm × 2 cm), and this was separated using a C18 analytical column (75 µm × 100 mm 3 µm, C18) through a 120-min gradient at a flow rate of 300 nl/min. The gradient used was set up as follows: 0–100 min, B phase, increased linearly from 0% to 55%; 110–115 min, B phase, increased linearly from 55% to 100%; 115–120 min, B phase, remained at 100%.

The peptides were analyzed with the Q-Exactive mass spectrometry system (Thermo Scientific, Bremen, Germany). The MS data were operated using the data-dependent top ten method and acquired over the range 300–1,800 m/z, with a mass resolution of 70,000 at 200 m/z. The dynamic exclusion duration was 40.0 s. Tandem mass spectrometry (MS/MS) scans were acquired with a mass resolution of 17,500 at 200 m/z, and the isolation window was 2 m/z. The normalized collision energy was set at 30 eV, and the underfill ratio was defined as 0.1%.

iTRAQ data and bioinformation analysis: The resulting MS/MS spectra were processed using the Mascot engine (Matrix Science, London, UK; version 2.2) and Proteome Discoverer 1.4 (Thermo Scientific; version 1.4). They were searched against the UniProt protein database for *Cavia porcellus*, which contained 20,435 sequences (release data 201610). For the protein identification, mass tolerance was set to 20 ppm for precursor ions and 0.1 Da for fragmented ions, with an allowance for max 2 missed cleavages in the trypsin digests. Oxidation (M) and iTRAQ 8-plex (Y) were the potential variable modifications, and carbamidomethyl (C), iTRAQ 8-plex (N-term), and iTRAQ 8-plex (K) were the fixed modifications. A decoy database was used to estimate and ensure that the false discovery rate (FDR) was less than 1%. The Student *t* test was used to compare the differences in protein expression between the control and myopia groups and calculate the p value. A 1.2-fold cut-off was set to determine the upregulated and downregulated proteins with $p<0.05$ [23].

To further analyze the functions of differentially expressed proteins, Gene Ontology (GO) mapping and annotation were analyzed using the Blast2GO system. The protein classification of cellular components, biologic processes, and molecular functions was performed based on the functional annotations using the GO terms. Hierarchical clustering (HCL) analysis of the quantitative data between the control and experiment groups was performed using Cluster 3.0 software and visualized using Java TreeView software. Ingenuity Pathway Analysis (IPA; Ingenuity Systems, Redwood City, CA) was used to determine the potential biologic pathway interactions of differently expressed proteins.

Quantitative real-time PCR (qRT-PCR): Total RNA was isolated from the scleral tissues in the FDM and control groups (n = 3, each group) using TRIzol reagent (Life Technologies, Carlsbad, CA), according to the manufacturer's instructions. Then, the RNA concentration was measured using a NanoDrop 1000 spectrophotometer (Thermo Fisher Scientific). Afterward, reverse transcription and quantitative real-time PCR were performed using a PrimeScript RT–PCR kit (Takara, Kusatsu, Japan). The PCR reaction parameters were set as follows: initial denaturation: 95 °C 30 s and 40 amplification cycles: 95 °C 30 s, 60 °C 30 s 9, and Applied Biosystems was used. The relative expression levels of the target genes (Table 1) were calculated using the $2^{-\Delta\Delta Ct}$ method, and normalized to the housekeeping gene *GAPDH*.

Table 1. Sequence of primer pairs based on the NCBI database.

Gene	Forward primer (5′-3′)	Reverse primer (5′-3′)	Product size (bp)
RhoA	CGCCTTTGGATACATGGAGT	CAAGACAAGGCACCCAGATT	124
Myosin IIB	TTGATGCCAAGTCCTCTGTCT	GTGACAGTAGCTCCGCCTTC	118
RAP1A	CGTGGGAAAGTCTGCTCTGA	CGCTCATCTTCCAGGTCACA	174
ACTN3	GGTCCGAAAGTTGGTGCCTA	GCCGGTCAATGTTGCTCTTG	91
GAPDH	TCAAGAAGGTGGTGAAGCAG	CGTCAAAAGTGGAAGAATGG	117

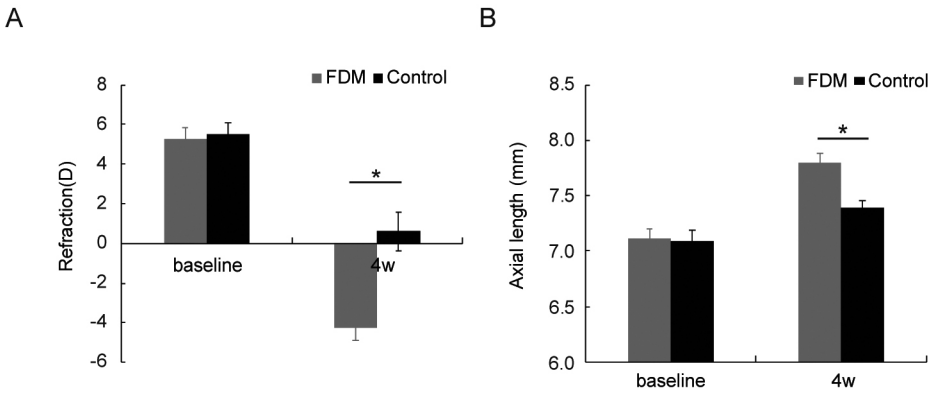

Figure 1. Refraction and axial length in control and FDM groups at the beginning and end of the treatment. **A**: Refraction and (**B**) axial length (n = 9, each group). Data are expressed as the mean ± standard deviation (SD). *p<0.05.

Western blotting: The proteins were extracted from sclera tissues in the FDM and control groups (n = 3, each group) using radioimmunoprecipitation assay (RIPA) lysis buffer containing the protease inhibitors. A total of 30 μg of proteins were subjected to SDS–polyacrylamide gel electrophoresis (SDS–PAGE) gels and transferred onto polyvinylidene difluoride (PVDF) membranes. After blocking for 1 h with TBS, which contained 0.1% Tween-20 (TBST) and 5% skim milk powder, the membranes were incubated with the primary antibody against myosin IIB (1:2,000, Abcam, Cambridge, UK), RhoA (1:1,000, CST, Beverly, MA), and GAPDH (1:5,000, Proteintech, Chicago, IL). Then, the membranes were rinsed with TBST three times and incubated with rabbit or mouse secondary antibodies conjugated to horseradish peroxidase (HRP) for 1 h at room temperature. Enhanced chemiluminescence (ECL) reagents (Amersham, Uppsala, Sweden) were used to develop the band according to the manufacturer's instructions.

Statistical analysis: Each experiment was performed at least in triplicate, and the values were expressed as mean ± standard deviation (SD). The refraction, axial length, and results of the qRT-PCR and western blotting of the FDM eyes were compared to those of the contralateral control eyes using the Student paired *t* test. SAS software (version 9.2, SAS Institute, Raleigh, NC) was used to perform the statistical evaluations. A p value of less than 0.05 was considered statistically significant.

RESULTS

Axial length and refraction changes: There was no statistically significant difference in refraction or axial length between the FDM group and the control group at the baseline (refraction: 5.25 ± 0.59 D versus 5.50 ± 0.67 D; axial length: 7.12 ± 0.08 mm versus 7.10 ± 0.09 mm; p>0.05; Figure 1). After 4 weeks, the form-deprivation eyes developed statistically significant degrees of myopia relative to the contralateral control eyes (−4.25 ± 0.61 D versus 0.61 ± 0.98 D; p<0.05; Figure 1A), and the axial length increased statistically significantly (7.79 ± 0.09 mm versus 7.39 ± 0.06 mm; p<0.05; Figure 1B).

Identification of differentially expressed proteins in sclera in myopic eyes: To identify proteins that are differentially expressed in the sclera in myopic eyes, quantitative proteomic analysis was performed on the form-deprivation and contralateral sclerae. The iTRAQ results identified a total of 196,581 spectra in the database, 20,483 matched spectra, 10,862 unique peptides, and 2,579 proteins with an FDR of <1%. Using a cut-off of 1.2-fold change and p<0.05, 140 proteins were identified to be differentially expressed between the sclerae in the myopic eyes and the control eyes. Among these 140 proteins, 56 proteins were upregulated, while 84 proteins were downregulated in the sclera in myopic eyes, when compared to the control group (Appendix 1 and Appendix 2). Figure 2A shows the hierarchical clustering, demonstrating the systematic variations (fold change >1.2, p<0.05) in the differentially expressed proteins between the FDM and control eyes. Volcano plots were generated using the fold-change values and p values, and revealed the relationship between fold change and the statistical significance. The vertical lines represent the 1.2-fold change (up and down, respectively), and the horizontal line corresponds to a p value of 0.05. The pink points in the plot represent the differentially expressed proteins that have statistical significance (Figure 2B).

Bioinformatics analysis of differentially expressed proteins in the FDM sclera: To gain insights into the biologic changes, GO analysis was performed to identify the statistically significantly enriched functional terms of differentially

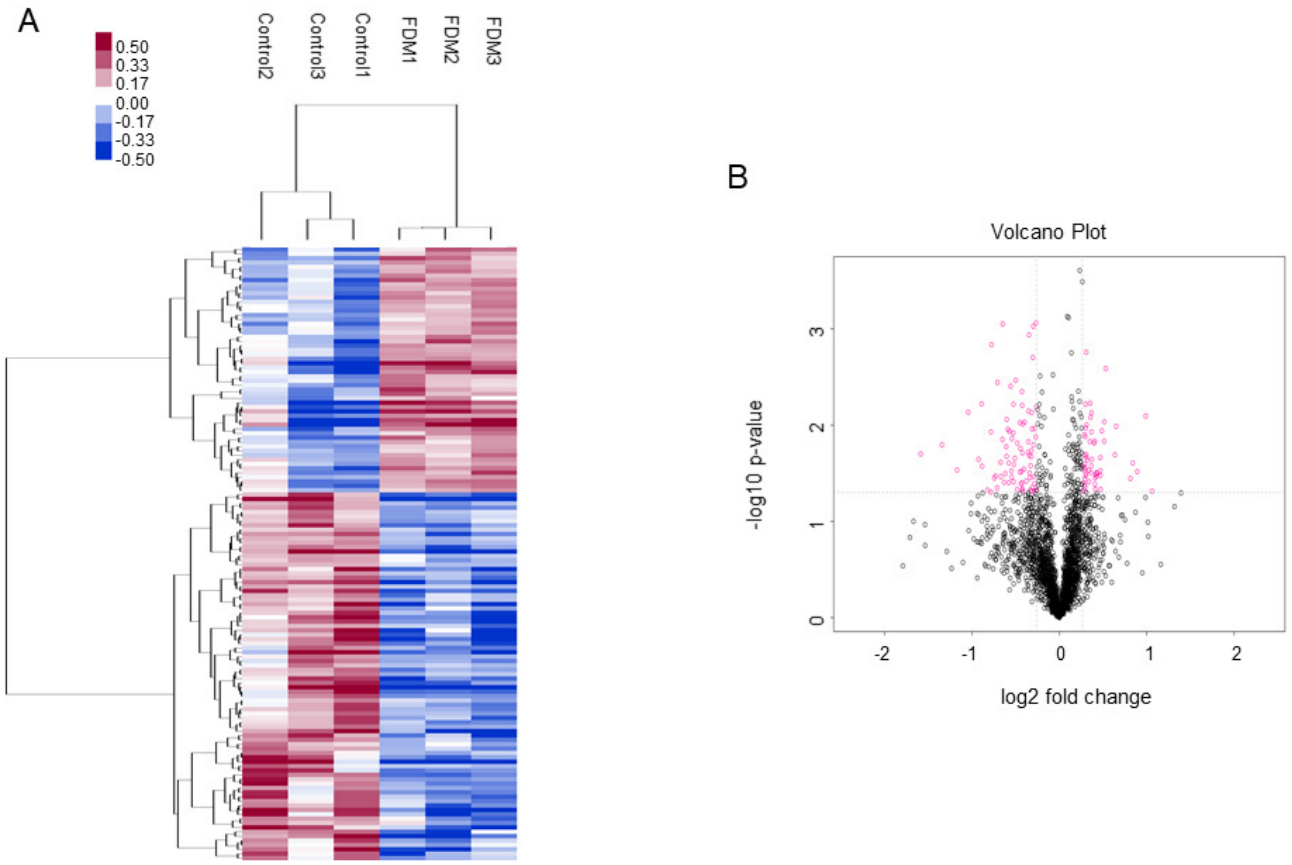

Figure 2. Global protein expression patterns in guinea pig sclera. **A**: Hierarchical clustering representation of total 140 differently expressed proteins. The magnitude of the percentage is represented by a color scale (top left) from low (blue) to high (red). **B**: Volcano plots representing the distribution of significance and fold change of differently expressed proteins in the form-deprivation myopia (FDM) group compared to the control group. Vertical lines represent 1.2-fold up and down, respectively, and the horizontal line corresponds to a p value of 0.05 (n = 3, each group).

expressed proteins. The 140 differentially expressed proteins were performed using three different criteria of protein functional annotation: biologic processes, molecular functions, and cellular components (Figure 3). The proteins involved in biologic processes, such as the cellular process (GO: 0009987), single-organism process (GO: 0044699), and metabolic process (GO: 0008152), were found to be altered in response to FDM (Figure 3A). Furthermore, the binding (GO: 0005488), catalytic activity (GO: 0003824), and transporter activity (GO: 0005215) of molecular functions were found to be involved in FDM (Figure 3B). For cellular components, the cell (GO: 0005623), cell part (GO: 0044464), and organelle (GO: 0043226) were correlated to sclera remodeling in FDM (Figure 3C). Figure 3D presents the number and percentage of proteins involved in the biologic processes, molecular functions, and cellular components.

The 140 differentially expressed proteins were further analyzed using IPA. According to the analysis of function and disease, 44 proteins were involved in cellular movement, and cellular assembly and organization (Figure 4A,B). The function of cellular assembly and organization can be further divided into five parts: organization of the cytoskeleton, microtubule dynamics, formation of the cytoskeleton, formation of filaments, and fibrogenesis (Figure 4C–G). Then, a sub-core analysis, which included cellular movement and cellular assembly and organization, was performed. The summary report revealed that the top five canonical pathways were glioma invasiveness signaling, germ cell–Sertoli cell junction signaling, production of nitric oxide and reactive oxygen species in macrophages, integrin-linked kinase (ILK) signaling, and integrin signaling (Figure 5A). The top five diseases and disorders were inflammatory response, cancer, hematological disease, immunological disease, and

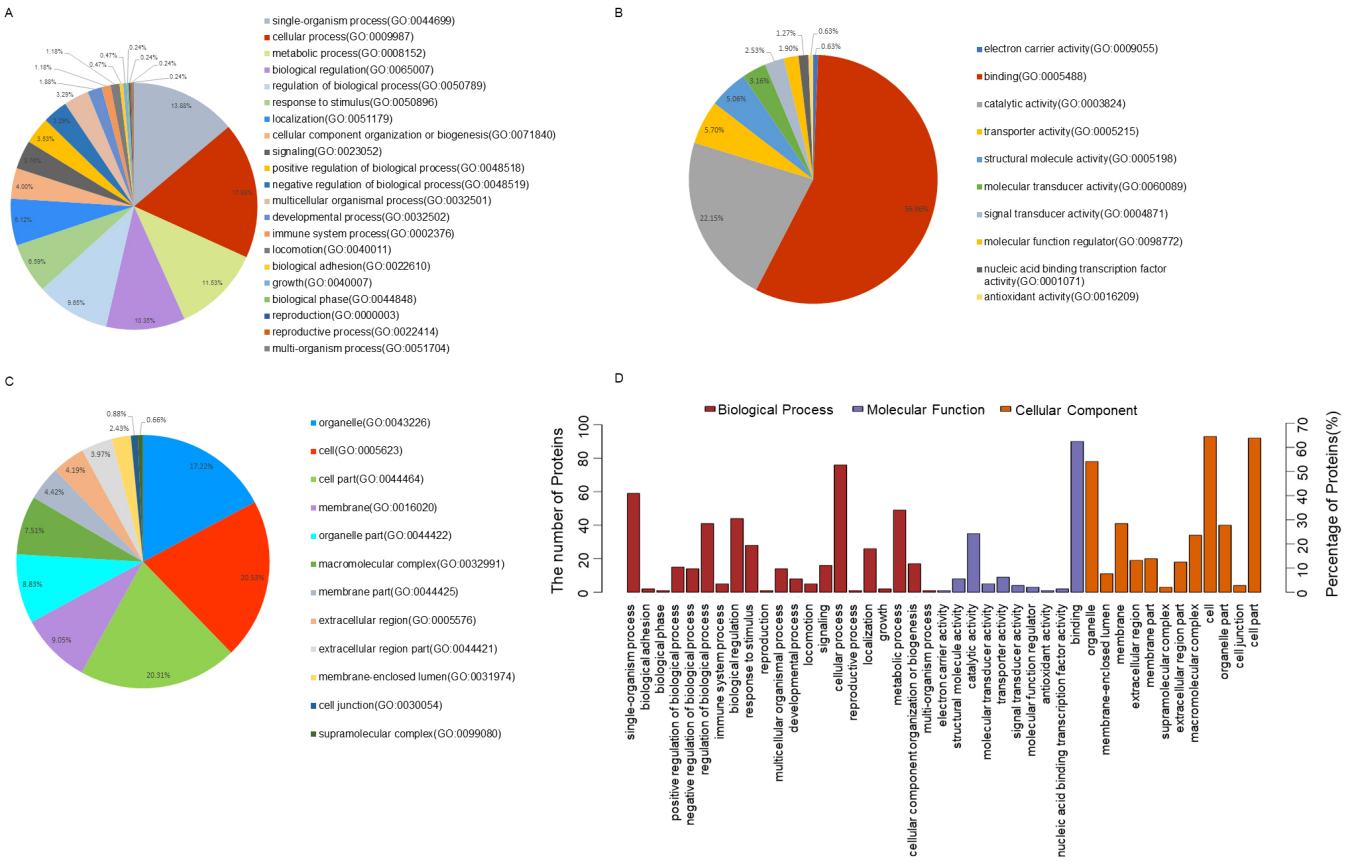

Figure 3. GO annotation and functional classification of differently expressed proteins. **A**: Biological process. **B**: Molecular functions. **C**: Cellular components. **D**: The summary of the number and percentage of proteins involved in biological process, molecular functions and cellular components.

organismal injury and abnormalities (Figure 5A). In addition, we created a sub-coexpression network, which included the ILK signaling and integrin signaling pathways. Figure 5B shows that these proteins are mainly correlated with RhoA.

Validation of differentially expressed proteins with qRT-PCR and western blotting: For any protein-encoding gene, alterations in the protein expression may be attributed to transcript changes. Thus, we performed an additional qRT-PCR to verify the differently expressed proteins discovered with iTRAQ. The results revealed that there was a decrease in the expression of myosin IIB and ACTIN3 and an increase in the expression of RAP1A and RhoA, which are consistent with the results obtained with iTRAQ (Figure 6A). The western blotting results revealed that myosin IIB decreased, while RhoA increased in the FDM group (Figure 6B–E). These findings suggest that the results of the proteomics in the present study are reliable.

DISCUSSION

In the present study, the iTRAQ proteomics strategy was performed to identify the differentially expressed proteins in sclera in myopic eyes. It was demonstrated that these differentially expressed proteins are mainly associated with cellular movement and cellular assembly and organization. Furthermore, the coexpression network revealed that RhoA plays a key role in the pathways of ILK signaling and integrin signaling, which are important pathways involved in cellular movement and cellular assembly and organization.

According to the IPA, the cytoskeleton plays an important role in modulating cellular assembly and organization. Myosin, which is one of the major cellular motor proteins, can regulate the cytoskeletal structure and function through its ability to bind with actin and hydrolyze ATP. Non-muscle myosin II (NMII) consists of six subunits, two myosin heavy chains (MHCs) and two pairs of myosin light chains (MLCs). Three MHC isoforms have been identified, namely, IIA, IIB,

and IIC. Each isoform has a specific cellular expression and functionality [24]. NMIIB has been proven to have the functions of regulation of cell shape, adhesion, and migration and contractility [25-28]. In the present study, it was found that there was a statistically significant decrease in NMIIB in sclera in myopic eyes. It was hypothesized that such cellular motor protein decrement may be correlated to the defect of contractility of the fibroblast, which further facilitates the sclera expansion and axial elongation. However, in the experimental glaucoma model, the level of myosin was higher and the axial length was larger, when compared to normal eyes [29]. Superficially, these results appeared to be inconsistent. In fact, the sclera underwent opposite changes in the condition of myopia and glaucoma, although the axial length presented an enlargement. This presented a thinner sclera and a decrease in mechanical compliance in eyes with myopia, and a thicker sclera and an increase in scleral stiffness in the eyes with glaucoma [30-32]. In addition, a previous

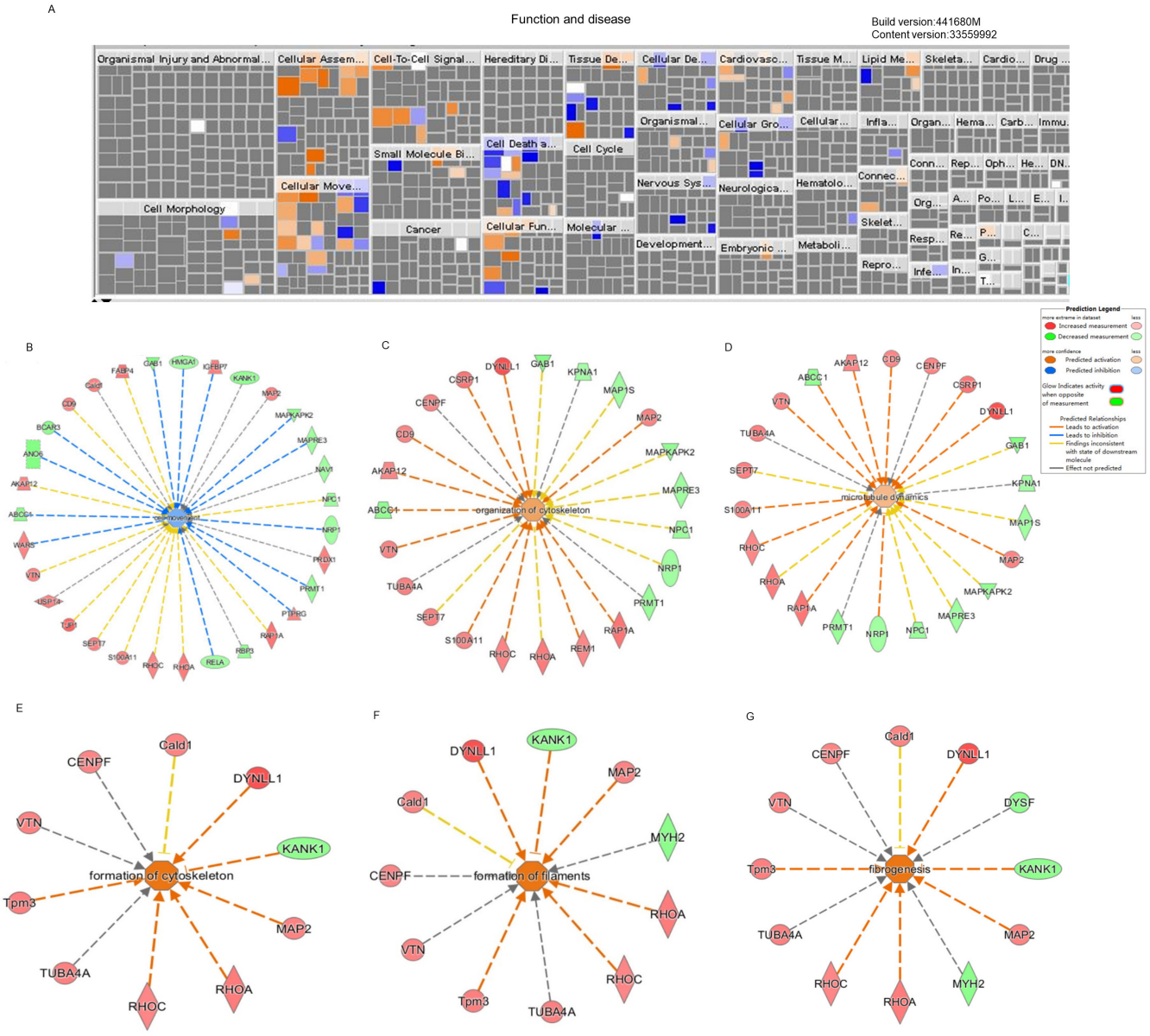

Figure 4. Protein function and network analysis using IPA. **A**: The function and disease analysis of differently expressed proteins. **B**: The network of cellular movement and cellular assembly and organization. **C**: Organization of cytoskeleton, **D**: microtubule dynamics, **E**: formation of cytoskeleton, **F**: formation of filaments, **G**: fibrogenesis. Red representing the upregulation proteins and green representing the downregulation proteins.

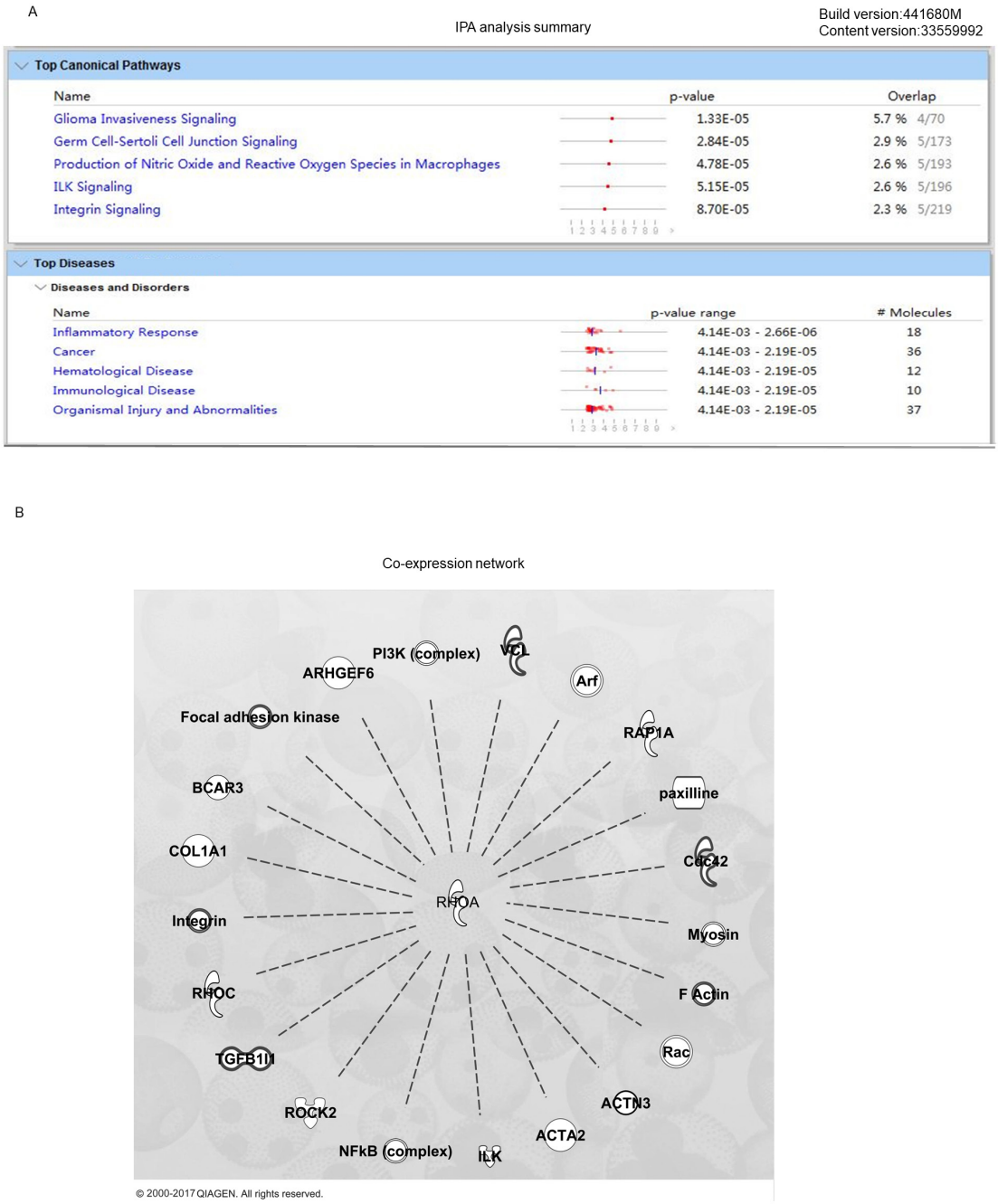

Figure 5. Canonical pathways and coexpression network using IPA. **A**: The top five canonical pathways and disease involved in cellular movement and cellular assembly and organization. **B**: The co-expression network of RhoA.

study revealed that myosin that decreased in the sclera of lens induced myopia [19]. The knockout of NMIIB in epicardial cells has been shown to impair epicardial integrity, which results in a compromised epicardial barrier function [33]. Furthermore, it was observed that there was a statistically significant reduction in the thickness of actin stress fibers in NMIIB-negative cells, when compared to those in wild-type cells. Therefore, NMIIB can regulate actin stress fiber formation during epicardial maturation. Furthermore, NMII also promotes the maturation of nascent focal adhesion complexes [34,35]. In primary foreskin fibroblasts, the inhibition of NMII is correlated to the marked reduction in vinculin, FAK, and α-actinin [35]. In the present study, there was also decreased expression of α-actinin in the sclera in myopic

eyes. Taken together, it was hypothesized that NMIIB may establish a link between integrins and the actin cytoskeleton, which plays an important role in sclera remodeling in myopic eyes [36].

IPA revealed that the ILK and integrin pathways are involved in cellular movement and cellular assembly and organization in scleral remodeling in myopic eyes. The role of RhoA is focused, as this is located in the core position in the IPA network analysis. It is known that the Ras homolog gene family has important regulators for a variety of cellular functions [37,38]. Among these regulators, RhoA has been shown to play a key role in the regulation of cellular morphology, adhesion and migration, and the transformation of cellular phenotypes [39]. The qRT-PCR and western blotting results confirmed that RhoA is upregulated in the sclera in myopic eyes. Previous studies have demonstrated the activation role of the RhoA signaling pathway in myofibroblast differentiation, which is characterized by the expression of α-smooth muscle actin (α-SMA). In a previous study, we found that there is increased expression of α-SMA in the sclera in myopic eyes, which is consistent with other studies [40-42]. The study conducted by Zhou showed that sclera myofibroblast differentiation, which results in an increase in α-SMA and a decrease in collagen deposition, is involved in sclera

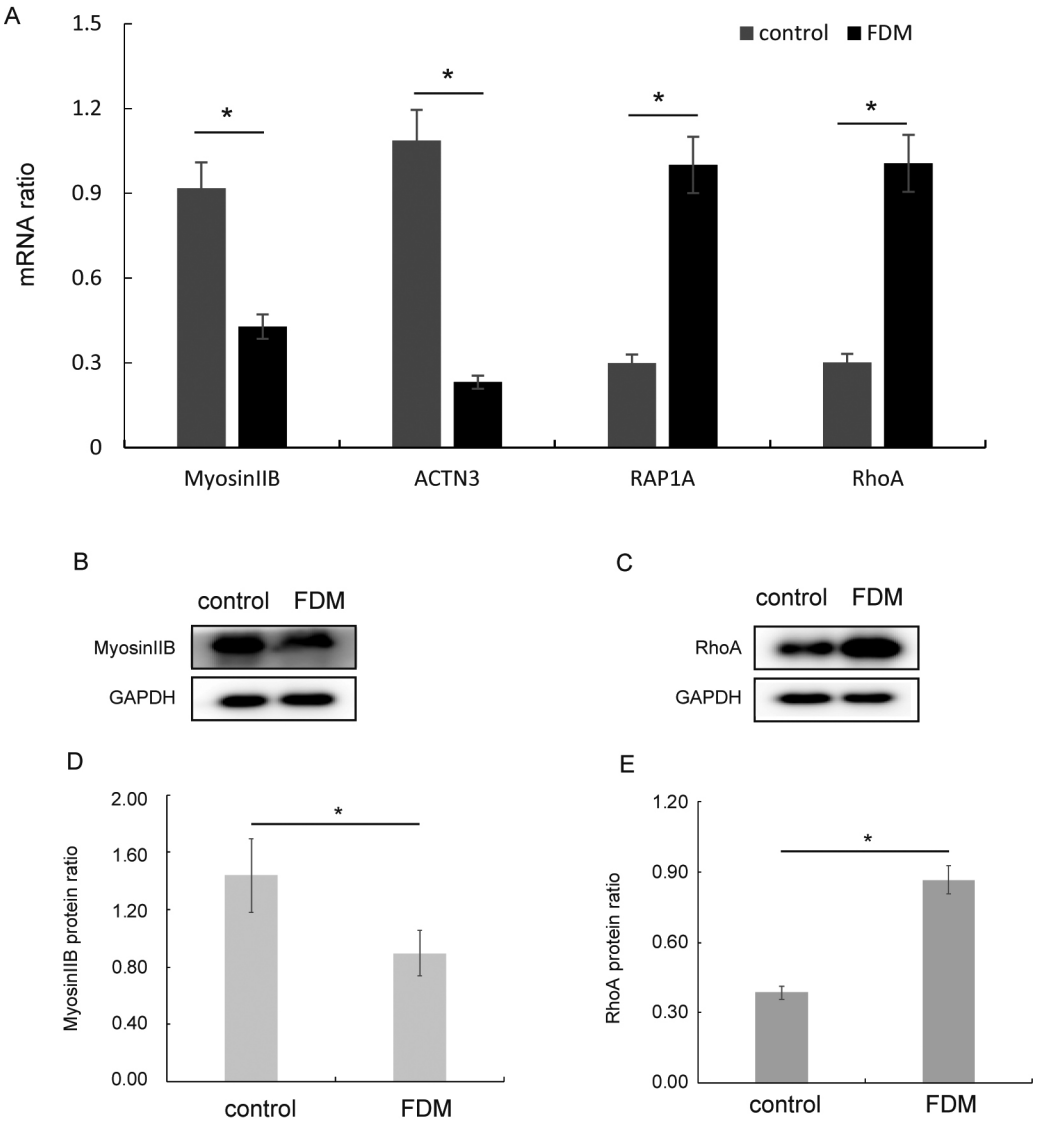

Figure 6. qRT-PCR analysis of myosin IIB, ACTIN3, RAP1A, and RhoA in the control and FDM groups (**A**, **B**, **C**, **D**, n = 3, each group). Western blotting of myosin IIB and RhoA in the control and form-deprivation myopia (FDM) groups (**E**, **F**, **G**, **H**, n = 3, each group). Data are expressed as the mean ± standard deviation (SD). *p<0.05.

remodeling in myopic eyes [41]. As a result, it was assumed that the upregulation of RhoA in the sclera in myopic eyes is correlated to scleral α-SMA expression. Meanwhile, RhoA was found to regulate the myosin assembly [43]. Furthermore, more studies have focused on factors that regulate RhoA activation. It has been well demonstrated that the activation of RhoA is correlated to mechanical stimulation, which was also confirmed by a previous study we conducted [40,44]. When cells are subjected to exogenous mechanical force, cell adhesion molecules, such as integrins, sense and transmit mechanical stimulations to the cytoskeleton, which further activates RhoA from the GDP-bound state to the GTP-bound state, inducing changes to the cytoskeleton, such as myosin assembly and α-SAM expression [45]. Therefore, we consider that RhoA activation was the result of the change in scleral strain, which plays an important role in the organization of the scleral cell cytoskeleton in myopia.

The present study focused on changes in the protein profiles of the sclera in myopic eyes of guinea pigs. Previously, Zhou et al. used 2DGE to compare differentially expressed proteins in the sclera of guinea pigs with myopia [46]. Zhou et al. found only 26 differently expressed proteins, which is not consistent with the results we have reported. This inconsistency may be related to the different methods and different ages of the guinea pigs. There were several limitations in the present study. Although the number of samples in the myopia group and the control group involved in the proteomic process was small, a confirmation experiment was conducted using different samples. The qRT-PCR and western blotting results were consistent with the proteomics, which suggests that the iTRAQ results are reliable. In addition, we mainly focused on the pathway and network of differently expressed proteins, providing insights into sclera remodeling during the development of myopia. Further studies are needed to confirm and explore the underlying mechanism.

APPENDIX 1. UPREGULATED PROTEIN EXPRESSION BETWEEN MYOPIA AND CONTROL SCLERA.

To access the data, click or select the words "Appendix 1."

APPENDIX 2. DOWNREGULATED PROTEIN EXPRESSION BETWEEN MYOPIA AND CONTROL SCLERA.

To access the data, click or select the words "Appendix 2."

ACKNOWLEDGMENTS

Grant/financial support: This work was supported by Grant 81,770,953 from National Natural Science Foundation, Grant 81,900,900 from National Natural Science Foundation, Grant ZH2018QNA18 from Translational Medicine Crossover Research Fund of Shanghai Jiao Tong University, Grant 2018ZHYL0222 from intelligent medical project of Shanghai, Grant 2020YFC2003904 from National Key Research & Development Program. Conflict of Interest: None of the authors of the manuscript has proprietary interest in any materials or methods described in this article.

REFERENCES

1. He M, Huang W, Zheng Y, Huang L, Ellwein LB. Refractive error and visual impairment in school children in rural southern China. Ophthalmology 2007; 114:374-82. [PMID: 17123622].

2. Rudnicka AR, Kapetanakis VV, Wathern AK, Logan NS, Gilmartin B, Whincup PH, Cook DG, Owen CG. Global variations and time trends in the prevalence of childhood myopia, a systematic review and quantitative meta-analysis: implications for aetiology and early prevention. Br J Ophthalmol 2016; 100:882-90. [PMID: 26802174].

3. McBrien NA, Cornell LM, Gentle A. Structural and ultrastructural changes to the sclera in a mammalian model of high myopia. Invest Ophthalmol Vis Sci 2001; 42:2179-87. [PMID: 11527928].

4. Jonas JB, Xu L. Histological changes of high axial myopia. Eye (Lond) 2014; 28:113-7. [PMID: 24113300].

5. Sergienko NM, Shargorogska I. The scleral rigidity of eyes with different refractions. Graefes Arch Clin Exp Ophthalmol 2012; 250:1009-12. [PMID: 22407293].

6. Avetisov ES, Savitskaya NF, Vinetskaya MI, Iomdina EN. A study of biochemical and biomechanical qualities of normal and myopic eye sclera in humans of different age groups. Metab Pediatr Syst Ophthalmol 1983; 7:183-8. [PMID: 6678372].

7. Grytz R, Siegwart JT. Changing material properties of the tree shrew sclera during minus lens compensation and recovery. Invest Ophthalmol Vis Sci 2015; 56:2065-78. [PMID: 25736788].

8. Watson PG, Young RD. Scleral structure, organisation and disease. A review. Exp Eye Res 2004; 78:609-23. [PMID: 15106941].

9. Bailey AJ. Structure function and ageing of the collagens of the eye. Eye (Lond) 1987; 1:175-83. [PMID: 3308525].

10. McBrien NA, Lawlor P, Gentle A. Scleral remodeling during the development of and recovery from axial myopia in the tree shrew. Invest Ophthalmol Vis Sci 2000; 41:3713-9. [PMID: 11053267].

11. Song Y, Zhang F, Zhao Y, Sun M, Tao J, Liang Y, Ma L, Yu Y, Wang J, Hao J. Enlargement of the Axial Length and Altered Ultrastructural Features of the Sclera in a Mutant Lumican Transgenic Mouse Model. PLoS One 2016; 11:e0163165-[PMID: 27711221].

12. Rada JA, Palmer L. Choroidal regulation of scleral glycosaminoglycan synthesis during recovery from induced myopia. Invest Ophthalmol Vis Sci 2007; 48:2957-66. [PMID: 17591860].

13. Yuan Y, Li M, Chen Q, Me R, Yu Y, Gu Q, Shi G, Ke B. Crosslinking Enzyme Lysyl Oxidase Modulates Scleral Remodeling in Form-Deprivation Myopia. Curr Eye Res 2018; 43:200-7. [PMID: 29135319].

14. Funata M, Tokoro T. Scleral change in experimentally myopic monkeys. Graefes Arch Clin Exp Ophthalmol 1990; 228:174-9. [PMID: 2338255].

15. Siegwart JT, Norton TT. Selective regulation of MMP and TIMP mRNA levels in tree shrew sclera during minus lens compensation and recovery. Invest Ophthalmol Vis Sci 2005; 46:3484-92. [PMID: 16186323].

16. Li M, Yuan Y, Chen Q, Me R, Gu Q, Yu Y, Sheng M, Ke B. Expression of Wnt/beta-Catenin Signaling Pathway and Its Regulatory Role in Type I Collagen with TGF-beta1 in Scleral Fibroblasts from an Experimentally Induced Myopia Guinea Pig Model. J Ophthalmol 2016; 2016:5126560-[PMID: 27247798].

17. Gentle A, McBrien NA. Retinoscleral Control of Scleral Remodelling in Refractive Development: A Role for Endogenous FGF-2? Cytokine 2002; 18:344-8. [PMID: 12160524].

18. Lam TC, Li KK, Lo SC, Guggenheim JA, To CH. Application of fluorescence difference gel electrophoresis technology in searching for protein biomarkers in chick myopia. J Proteome Res 2007; 6:4135-49. [PMID: 17924678].

19. Frost MR, Norton TT. Alterations in protein expression in tree shrew sclera during development of lens-induced myopia and recovery. Invest Ophthalmol Vis Sci 2012; 53:322-36. [PMID: 22039233].

20. Mertins P, Udeshi ND, Clauser KR, Mani DR, Patel J, Ong SE, Jaffe JD, Carr SA. iTRAQ labeling is superior to mTRAQ for quantitative global proteomics and phosphoproteomics. Mol Cell Proteomics 2012; 11:M111-[PMID: 22210691].

21. Aggarwal K, Choe LH, Lee KH. Shotgun proteomics using the iTRAQ isobaric tags. Brief Funct Genomics Proteomic 2006; 5:112-20. [PMID: 16772272].

22. Barathi VA, Chaurasia SS, Poidinger M, Koh SK, Tian D, Ho C, Iuvone PM, Beuerman RW, Zhou L. Involvement of GABA transporters in atropine-treated myopic retina as revealed by iTRAQ quantitative proteomics. J Proteome Res 2014; 13:4647-58. [PMID: 25211393].

23. Wu Y, Lam CS, Tse DY, To CH, Liu Q, McFadden SA, Chun RK, Li KK, Bian J, Lam C. Early Quantitative Profiling of Differential Retinal Protein Expression in Lens-Induced Myopia in Guinea Pig Using Fluorescence Difference Two-Dimensional Gel Electrophoresis. Mol Med Rep 2018; 17:5571-80. [PMID: 29436656].

24. Conti MA, Adelstein RS. Nonmuscle myosin II moves in new directions. J Cell Sci 2008; 121:11-8. [PMID: 18096687].

25. Gutzman JH, Sahu SU, Kwas C. Non-muscle myosin IIA and IIB differentially regulate cell shape changes during zebrafish brain morphogenesis. Dev Biol 2015; 397:103-15. [PMID: 25446029].

26. Ma X, Jana SS, Conti MA, Kawamoto S, Claycomb WC, Adelstein RS. Ablation of nonmuscle myosin II-B and II–C reveals a role for nonmuscle myosin II in cardiac myocyte karyokinesis. Mol Biol Cell 2010; 21:3952-62. [PMID: 20861308].

27. Chi Q, Yin T, Gregersen H, Deng X, Fan Y, Zhao J, Liao D, Wang G. Rear actomyosin contractility-driven directional cell migration in three-dimensional matrices: a mechano-chemical coupling mechanism. J R Soc Interface 2014; 11:20131072-[PMID: 24647903].

28. Bond JE, Ho TQ, Selim MA, Hunter CL, Bowers EV, Levinson H. Temporal spatial expression and function of non-muscle myosin II isoforms IIA and IIB in scar remodeling. Lab Invest 2011; 91:499-508. [PMID: 21102503].

29. Oglesby EN, Tezel G, Cone-Kimball E, Steinhart MR, Jefferys J, Pease ME, Quigley HA. Scleral fibroblast response to experimental glaucoma in mice. Mol Vis 2016; 22:82-99. [PMID: 26900327].

30. McBrien NA, Jobling AI, Gentle A. Biomechanics of the sclera in myopia: extracellular and cellular factors. Optom Vis Sci 2009; 86:E23-30. [PMID: 19104466].

31. Nguyen C, Cone FE, Nguyen TD, Coudrillier B, Pease ME, Steinhart MR, Oglesby EN, Jefferys JL, Quigley HA. Studies of scleral biomechanical behavior related to susceptibility for retinal ganglion cell loss in experimental mouse glaucoma. Invest Ophthalmol Vis Sci 2013; 54:1767-80. [PMID: 23404116].

32. Gottanka J, Flugel-Koch C, Martus P, Johnson DH, Lutjen-Drecoll E. Correlation of pseudoexfoliative material and optic nerve damage in pseudoexfoliation syndrome. Invest Ophthalmol Vis Sci 1997; 38:2435-46. [PMID: 9375560].

33. Ma X, Sung DC, Yang Y, Wakabayashi Y, Adelstein RS. Nonmuscle myosin IIB regulates epicardial integrity and epicardium-derived mesenchymal cell maturation. J Cell Sci 2017; 130:2696-706. [PMID: 28687623].

34. le Duc Q, Shi Q, Blonk I, Sonnenberg A, Wang N, Leckband D, de Rooij J. Vinculin potentiates E-cadherin mechanosensing and is recruited to actin-anchored sites within adherens junctions in a myosin II-dependent manner. J Cell Biol 2010; 189:1107-15. [PMID: 20584916].

35. Pasapera AM, Schneider IC, Rericha E, Schlaepfer DD, Waterman CM. Myosin II activity regulates vinculin recruitment to focal adhesions through FAK-mediated paxillin phosphorylation. J Cell Biol 2010; 188:877-90. [PMID: 20308429].

36. Choi CK, Vicente-Manzanares M, Zareno J, Whitmore LA, Mogilner A, Horwitz AR. Actin and alpha-actinin orchestrate the assembly and maturation of nascent adhesions in a myosin II motor-independent manner. Nat Cell Biol 2008; 10:1039-50. [PMID: 19160484].

37. Asparuhova MB, Gelman L, Chiquet M. Role of the actin cytoskeleton in tuning cellular responses to external mechanical stress. Scand J Med Sci Sports 2009; 19:490-9. [PMID: 19422655].

38. Korol A, Taiyab A, West-Mays JA. RhoA/ROCK signaling regulates TGFbeta-induced epithelial-mesenchymal transition of lens epithelial cells through MRTF-A. Mol Med 2016; 22:713-23. [PMID: 27704140].

39. Heasman SJ, Ridley AJ. Mammalian Rho GTPases: new insights into their functions from in vivo studies. Nat Rev Mol Cell Biol 2008; 9:690-701. [PMID: 18719708].

40. Yuan Y, Li M, To CH, Lam TC, Wang P, Yu Y, Chen Q, Hu X, Ke B. The Role of the RhoA/ROCK Signaling Pathway in Mechanical Strain-Induced Scleral Myofibroblast Differentiation. Invest Ophthalmol Vis Sci 2018; 59:3619-29. [PMID: 30029249].

41. Wu H, Chen W, Zhao F, Zhou Q, Reinach PS, Deng L, Ma L, Luo S, Srinivasalu N, Pan M, Hu Y, Pei X, Sun J, Ren R, Xiong Y, Zhou Z, Zhang S, Tian G, Fang J, Zhang L, Lang J, Wu D, Zeng C, Qu J, Zhou X. Scleral hypoxia is a target for myopia control. Proc Natl Acad Sci USA 2018; 115:E7091-100. [PMID: 29987045].

42. Wu PC, Tsai CL, Gordon GM, Jeong S, Itakura T, Patel N, Shi S, Fini ME. Chondrogenesis in scleral stem/progenitor cells and its association with form-deprived myopia in mice. Mol Vis 2015; 21:138-47. [PMID: 25684979].

43. Kamijo K, Ohara N, Abe M, Uchimura T, Hosoya H, Lee JS, Miki T. Dissecting the role of Rho-mediated signaling in contractile ring formation. Mol Biol Cell 2006; 17:43-55. [PMID: 16236794].

44. Marjoram RJ, Lessey EC, Burridge K. Regulation of RhoA activity by adhesion molecules and mechanotransduction. Curr Mol Med 2014; 14:199-208. [PMID: 24467208].

45. Hu S, Cui D, Yang X, Hu J, Wan W, Zeng J. The crucial role of collagen-binding integrins in maintaining the mechanical properties of human scleral fibroblasts-seeded collagen matrix. Mol Vis 2011; 17:1334-42. [PMID: 21647271].

46. Zhou X, Ye J, Willcox MD, Xie R, Jiang L, Lu R, Shi J, Bai Y, Qu J. Changes in protein profiles of guinea pig sclera during development of form deprivation myopia and recovery. Mol Vis 2010; 16:2163-74. [PMID: 21139681].

Articles are provided courtesy of Emory University and the Zhongshan Ophthalmic Center, Sun Yat-sen University, P.R. China. The print version of this article was created on 1 September 2021. This reflects all typographical corrections and errata to the article through that date. Details of any changes may be found in the online version of the article.